Asian Journal of Civil Engineering
https://doi.org/10.1007/s42107-020-00282-8

ORIGINAL PAPER

# Black Hole Mechanics Optimization: a novel meta-heuristic algorithm

**A. Kaveh**[1] · **M. R. Seddighian**[1] · **E. Ghanadpour**[1]

Received: 11 June 2020 / Accepted: 6 July 2020


**Abstract**
In this paper, a new meta-heuristic algorithm is proposed. The proposed method contains a mathematical kernel and a physical simulation. The mathematical kernel computes the optimum direction of each variable subjected to the cost function. Then, it conducts generated data to the detected path. Besides, the physical simulation controls the exploration procedure as well as the exploitation. The simulating process is based on the mechanics of black holes. In the structure of the proposed algorithm, there are two types of black holes. The first is a Kerr black hole forming a circular gravity filed to explore all the problem search space. The other one is a Schwarzschild black hole exploiting the data in the vicinity of its singularity. Eventually, the potency and efficiency of the new algorithm are investigated using several mathematical and four benchmark skeletal structures.

**Keywords** Optimization · Meta-heuristic algorithms · Black hole mechanics · Covariance matrix · Optimum design

## Introduction

Optimization is a process that finds the best available solution from all the feasible ones. The subject is divided into various branches such as mathematical approaches and meta-heuristic algorithms. The mathematical programming method usually converges to the analytically exact optimum solution. However, they require gradient information and an appropriate starting point to perform correctly, preventing trapping in local optimums (Kaveh and Mahdavi 2013). These methods fail their competence when the problem considered becomes more complex, increasing the total cost of the solution. A problem is called NP-complete when the set of all feasible solutions cannot be found in polynomial time on a non-deterministic Turing machine. In NP-complete problems, it is more efficient to utilize the meta-heuristic algorithms to obtain optimum or sub-optimum solutions subjected to specified constraints (Garey and Johnson 1979).

Meta-heuristic algorithms are proper tools for dealing with discontinuous, non-smooth, complex, and NP-complete problems. They can find acceptable global or near-global solutions with reasonable computational efforts (Talbi 2009). These algorithms have confirmed their efficiency in a wide range of fields. Nature-inspired meta-heuristic algorithms benefit from the metaphors of (1) evolutionary concepts, (2) swarm intelligence, or (3) physical laws. Evolution-based methods are inspired by the laws of natural evolutions. Genetic Algorithm (GA) (Holland 1992), Differential Evolution (DE) (Storn and Price 1997), and Evolution Strategy (ES) (Rechenberg 1978) can be named as the most popular algorithms from this category. Swarm-based algorithms are stochastic search methods that imitate the social behavior of natural or artificial species. Kennedy and Eberhart (1995) established the Particle Swarm Optimization (PSO) that mimics animal flocking behaviors. The Ant Colony Optimization (ACO), proposed by Dorigo et al. (1996) follows the process of finding the closest path for a source food in an ant colony. The navigation ability of dolphins was simulated in Dolphin Echolocation (DE) by Kaveh and Farhoudi (2013). The Artificial Bee Colony (ABC) developed by Karaboga and Basturk (2007) based on Bee's natural behavior. The introduced algorithms are some of the most well-known swarm algorithms. As more instances for swarm-based techniques, it is possible to list other methods as Monkey search (Mucherino and Seref 2007), Cuckoo Search (CS) (Yang and Deb 2009), Bat Algorithm (BA) (Yang 2010a), Firefly Algorithm (FA) (Yang 2010b), Bird Mating Optimizer (BMO) (Askarzadeh and Rezazadeh 2013), Krill Herd (KH) (Gandomi and Alavi

✉ A. Kaveh
alikaveh@iust.ac.ir

[1] School of Civil Engineering, Iran University of Science and Technology, Narmak, 16846-13114 Tehran, Iran

Published online: 13 July 2020

2012), Grey Wolf Optimizer (GWO) (Mirjalili et al. 2014), Ant Lion Optimizer (ALO) (Mirjalili 2015) and Whale Optimization Algorithms (WOA) (Mirjalili and Lewis 2016). Another category is physical-based techniques which are inspired by physical laws such as Simulated Annealing (SA) (Kirkpatrick et al. 1983), Tabu search (TS) (Glover 1989), Harmony Search (HS) (Geem et al. 2001), Big-Bang Big-Crunch (BBBC) (Erol and Eksin 2006), Galaxy-based Search Algorithm (GSA) (Shah-Hosseini 2011) and Water Cycle Algorithm (WCA) (Eskandar et al. 2012). Furthermore, there are some newer algorithms in the mentioned branch, such as Charged System Search (CSS) proposed by Kaveh and Talatahari (2010a) in which the governing Coulomb law from electrostatics and the Newtonian laws of mechanics are employed. Kaveh and Khayatazad (2012) developed Ray Optimization (RO) based on Snell's light refraction law. Colliding Bodies Optimization, (CBO) introduced by Kaveh and Mahdavi (2015), employs the laws of collisions between bodies. Kaveh and Bakhshpoori (2016) proposed the Water Evaporation Optimization (WEO) that mimics the evaporation of a tiny amount of water molecules. Vibrating Particles System (VPS) presented by Kaveh and Ilchi Ghazaan (2017) imitates single degree of freedom free vibration systems with viscous damping. Also, some researchers (Mirjalili and Lewis 2016) considered another category for meta-heuristic methods, which is according to the inspiration of human behavior in diverse fields such as Imperialist Competitive Algorithm (ICA) (Atashpaz-Gargari and Lucas 2007), Teaching–Learning-based Optimization (TLBO) (Rao et al. 2011), Soccer League Competition (SLC) algorithm (Moosavian and Kasaee 2014), and Tug of War Optimization (TWO) (Kaveh 2017).

Meta-heuristic methods are utilized in broad fields, including structural engineering. Many algorithms have been established to deal with structural optimization problems, which are examples of the most challenging topics of researchers' investigations. Cascade Enhanced Colliding Body Optimization is employed by Kaveh and BolandGerami (2016) to overcome the complexity of optimal design of large-scale steel frames. Kaveh and Ilchi Ghazaan (2016) illustrated the capability of Enhanced Whale Optimization Algorithm (EWOA) in the sizing optimization of skeletal structures. In the following, Kaveh et al. (2015) developed an improved version of magnetic charged system search for optimization of truss structures with continuous and discrete variables. Efficiency of a modified Genetic Programming (GP) according to Knowledge Discovery is verified in multi-objective optimization problems (Russo et al. 2017). Hasancebi and Kazemzadeh Azad (2015) presented a novel meta-heuristic algorithm which is called adaptive dimensional search for discrete truss sizing optimization. A Craziness based Particle Swarm Optimization is adopted in dealing with truss optimization with respect to frequency constraints (Carvalho et al. 2017). The competency of the Jaya algorithm is demonstrated in structural damage identification problems based on the determination of the sites and extent of damage (Du et al. 2018). Kazemzaeh Azad (2019) proposed monitored convergence curve as a new framework for meta-heuristic structural optimization algorithm. Truong and Kim (2018) studied the performance of a differential evolution-based method in reliability design optimization of nonlinear inelastic trusses. Iterative Topographical Global Optimization (ITGO) is utilized in establishing a new method to solve nonlinear constrained optimization problems (Ferreira et al. 2018). Kaveh et al. (2019) presented a chaotic Firefly Algorithm based on Gaussian map for the optimum design of large steel skeletal structures. Also, Kaveh and Ilchi (2015) presented a comparative study of the CBO and the ECBO algorithms for optimal design of skeletal structures. A Guided Population Archive Whale Optimization Algorithm based on Pareto dominance is introduced for solving multi-objective optimization problems (Got et al. 2019). In the work of Latif and Saka (2019), an enhanced version of Artificial Bee Colony (ABC) algorithm was used in optimum design of tied-arch bridges due to AASHTO-LRFD Bridge Design Specifications. Tejani et al. (2019) employed modified adaptive symbiotic organisms search in dealing with multi-objective structural optimization. Kaveh et al. (2012) developed performance-based multi-objective optimization to optimize the large steel structures. A new Experience-Based Learning (EBL) algorithm was introduced for vibration-based structural damage identification by Zheng et al. (2019). The superiority of the Social Mimic Optimization (SMO) algorithm is shown in some engineering design problems (Balochian and Baloochian 2019).

All the mentioned algorithms are successful and influential in their scopes. Also, all of them can obtain acceptable solutions after some iterations. However, it seems that some changes in their approaches will lead to more efficient and appropriate performance. For instance, none of them consider the orientation of candidate solutions due to their relative cost in search space. In other words, the best direction for increasing or decreasing candidate solutions has not been considered in their strategies. Therefore, this weak point leads to random improvement, which consumes a high level of costs, including time and memory. Since all generated data contributes to the calculation of the direction of the population tendency, the solutions that are generated inadequately, should be eliminated in each step. This property can improve the potency of the algorithm in finding the best solution. Another shortcoming of the previous algorithms is the type of population update. If a proper point can be found in which the global best solution is surmised in the vicinity of it, then it will be more economical to generate new data in its proximity.

In this paper, a new meta-heuristic algorithm is developed in which its mathematical kernel conducts the exploration and exploitation procedures. This leads to finding the best solution by spending lower costs (time and memory) in the problem-solving procedure. Besides the mathematical kernel, the physical simulation theory (based on black hole mechanics and entropy) controls some other drawbacks, which seem to exist in the other algorithms.

The rest of the paper is structured as follows: "Black Hole Mechanics Optimization" is presented first. Computational aspects of the developed algorithm are elaborated in "Computational details". The BHMO algorithm is employed to solve different types of problems in "Examples". Finally, "Concluding remarks" concludes the study and suggests some directions for future studies.

## Black Hole Mechanics Optimization

As mentioned in the introduction, despite the propensity of well-known meta-heuristic algorithms in solving various types of problems, there are some weak points in their procedures which impose more expenditure on their applications.

Black Hole Mechanics Optimization (BHMO) is a new meta-heuristic algorithm that is developed to improve the mentioned drawbacks of the previous methods. BHMO employs a robust mathematical kernel based on covariance matrix formed between each variable and its relative cost. This covariance matrix leads to finding the optimum orientation for increasing or decreasing the current variable. By this technique, each variable is directed rapidly toward its relative best value. Moreover, each variable is assumed independently of the others in comparison with the cost function. This property leads to escaping from the local optimums that is present in the search space of some problems.

Besides the mathematical kernel, a physical simulation helps in conducting the variables in each step. This physical simulation that is based on black hole mechanics updates the variables in the vicinity of the surmised global best in each step. Also, the elimination of weak variables is due to physical simulation after total navigation by the mathematical kernel.

### Physical simulation

In essence, nature is usually seeking to reduce all kinds of costs in the procedure of minimum value investigation at an equilibrium state. The principles of minimum total potential energy and heat transfer synthesis between physical systems, which are considered as two fundamental concepts in engineering and mechanics, are well-known evidence for this claim. Therefore, a number of physical rules in the universe can lead to achieve optimal patterns and solutions. This phenomenon can also be discovered in the galaxy, where a black hole impresses space–time mechanics. A black hole indicates such attractive behavior involving many researchers in its legendary mechanics over the centuries. Its different mechanical behavior to absorb the stars and other astronomical objects may inspire to elicit an appropriate standpoint about contiguous conduction, which can be applied to the procedure of a meta-heuristic algorithms.

Stars, which are more than three times the Sun's mass, may collapse and continue to compress when they are at the end of their lives. Albert Einstein's general theory of relativity predicted that the deformation of space–time, which leads to the formation of a black hole, can take place when a mass is compacted sufficiently (Wald 1999; Taylor and Wheeler 2000). As a result of this compression, a black hole has a strong gravitational attraction that even electromagnetic radiation, such as light, is not able to escape from it. The boundary of such a region is called the event horizon. A black hole is invisible due to reflecting no light (Schutz 2003; Davies 1978), therefore it acts like an ideal black body. Also, based on quantum field theory in curved space–time, the black hole Hawking radiation spectrum is the same as a black body with its temperature being inversely proportional to its mass (Hawking and Ellis 1974a, b). The center of a black hole is known as its singularity, where the mass is concentrated. In other words, it is a region where the space–time curvature becomes infinitive (Carroll 2019). In the case of a Schwarzschild black hole (will be defined in the following), falling objects are carried to their singularity (Lewis and Kwan 2007).

According to the second law of black hole mechanics and assuming the weak energy condition, the horizon of a black hole is a non-decreasing function of time (Hawking and Ellis 1971).

$$\frac{\mathrm{d}A}{\mathrm{d}t} \geq 0, \tag{1}$$

where $A$ is the area of the event horizon.

It is similar to the second law of thermodynamics, which states that the total entropy of an isolated system can never decrease. Bekenstein suggested that a black hole should have an entropy proportional to its horizon (Wald 2001). On the other hand, Hawking radiation seems to violate the second law of black hole mechanics, since it carries away the entropy. It can be proved that the sum of the entropy of the matter surrounding a black hole and one-quarter of the area of the horizon is always increasing (Wald 2001; Hawking and Ellis 1990). Thus, Bekenstein–Hawking formula for the entropy of a black hole (Bekenstein 1973; Hawking and Ellis 1974a, b) can be stated as:

$$S_{\mathrm{BH}} = \frac{K_B A}{4L_P^2}, \tag{2}$$

where $K_{B,}$ $A$, and $L_P$ stand for the Boltzmann constant, area of the event horizon, and the Planck length, respectively.

The Boltzmann constant relates the average relative kinetic energy of particles in a gas with the temperature of the gas, which is defined as (Kalinin and Kononogov 2005):

$$K_B = \frac{R}{N_A} = 1.380649 \times 10^{-23}\mathrm{kg} \times \mathrm{m}^2 \cdot \mathrm{K}^{-1} \cdot \mathrm{s}^{-2}, \tag{3}$$

where $R$ is the gas constant and $N_A$ is equal to the number of particles in one mole.

The Planck length is the distance light travels in one unit of Planck time, which is equal to (Planck 1899):

$$L_P = \sqrt{\frac{\hbar G}{c^3}} = 1.616252 \times 10^{-35}\mathrm{m}, \tag{4}$$

where $\hbar$ is the reduced Planck constant, $G$ is Newton's gravity constant, and $c$ is the speed of light.

For four-dimensional space–times, the shape of the event horizon of a black hole is always approximately spherical (Hawking and Ellis 1973). For non-rotating (static) black holes, the shape of the event horizon is accurately spherical, while for rotating black holes (another type) the event horizon is oblate (Shapiro et al. 1995). The geometry of the event horizon of different types of black holes is illustrated in Fig. 1.

The properties of the black hole can be defined by Eqs. (5)–(7).

$$A = 4\pi(r_+^2 + a^2), \tag{5}$$

$$r_\pm = M \pm \sqrt{M^2 - a^2 - Q^2}, \tag{6}$$

$$a = \frac{J}{M}, \tag{7}$$

where $M$, $J$, and $Q$ are the mass, angular momentum, and charge of the black hole. In terms of the introduced properties, there exist four types of black holes as mentioned in Table 1.

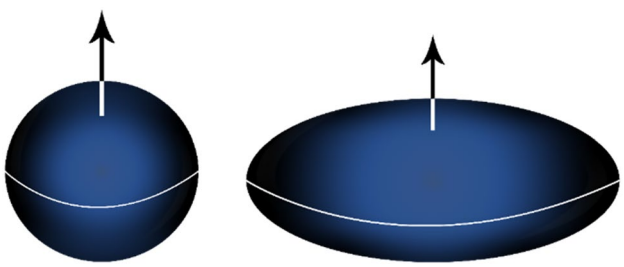

**Fig. 1** The geometry of the event horizon of different types of black holes

For a Kerr black hole, angular momentum is proportional to the moment of inertia $I$ and angular speed $\omega$.

$$J = I\omega. \tag{8}$$

In most cases for ablating spheroids, this is expressed as follows:

$$I = \frac{2}{5}\mathrm{MR}^2(1+\varepsilon), \tag{9}$$

$$\varepsilon = \frac{\alpha + \beta}{\alpha}, \tag{10}$$

where ε is the factor of ellipticity and $\alpha$ is the long radius, while $\beta$ is the short radius of the spheroid and $R$ is the elongated equatorial radius.

Also, for circular motion, it can be stated as in Eq. (11):

$$\omega = \frac{v}{r}, \tag{11}$$

therefore:

$$v = \frac{J}{\frac{2}{5}\mathrm{MR}(1+\varepsilon)}. \tag{12}$$

These equations and the type of absorption of particles into the black holes can be used as an inspiration to guide possible solutions in the search space to the global optimum.

## Mathematical kernel

In a number of meta-heuristic algorithms, the initial solutions are generated randomly in the search space. While attempting to find a reasonable connection between the produced solutions and the objective function as an essential issue requires attention. In other words, discovering how the change of the variables affects the objective function can lead to successfully raise data convergence speed to the optimum. Generally, figuring out that increasing of a variable has a direct or indirect relation with the objective function is imperative. It can help to improve the process of solving, which applies to a wide range of problems. Nevertheless, it is independent of the relationship between the current variables and others, which can prevent trapping in local optima.

**Table 1** The four types of black holes based on $Q$ and $J$

| | Non-rotating ($J=0$) | Rotating ($J>0$) |
|---|---|---|
| Uncharged ($Q=0$) | Schwarzschild | Kerr |
| Charged ($Q\neq0$) | Reissner–Nordström | Kerr–Newman |

In statistics and theory of probability, covariance is a measure of how much two random variables change together (Rice 2006). A positive covariance means that the two variables tend to move together, while two variables move inversely if and only if their relative covariance is negative. In the case of two jointly distributed real-valued random variables, the covariance of $X$ and $Y$ are defined by (Park 2018):

$$\mathrm{cov}(X, Y) = E\left[(X - E(X))\,(Y - E(Y))\right], \tag{13}$$

where $E(X)$, $E(Y)$ are the expected values of $X$ and $Y$, respectively.

The covariance matrix is a square and symmetric matrix given by:

$$C_{ij} = \mathrm{Cov}(X_i, X_j), \quad C \in \mathbb{R}^d, \tag{14}$$

where $d$ is the number of problem dimension.

For two-dimensional problems, it can be written as:

$$C = \begin{pmatrix} \mathrm{Cov}(X,X) & \mathrm{Cov}(X,Y) \\ \mathrm{Cov}(Y,X) & \mathrm{Cov}(Y,Y) \end{pmatrix}. \tag{15}$$

The direction of the main directions corresponds to the eigenvectors of the covariance matrix and relative lengths to the eigenvalue square roots of $x$.

Eigendecomposition of the covariance matrix leads to:

$$C = \mathrm{VLV}^{-1}, \tag{16}$$

where all the eigenvectors are put into the columns of matrix $V$. Also, all the eigenvalues are the entries of a diagonal matrix.

Linear transformation of the data set $X$ can be calculated by Eq. (17).

$$Y = TX, \tag{17}$$

where $T$ is the transformation matrix, and $Y$ represents the transformed data.

The transformation matrix is composed of a rotation matrix $R$ and a scaling matrix $S$ as follows:

$$T = RS. \tag{18}$$

By comparison to the decomposed form of matrix $C$, Eqs. (19), and (20) can be derived as:

$$C = RSSR^{-1}, \tag{19}$$

$$S = \sqrt{L}, \quad R = V. \tag{20}$$

Therefore,

$$T = V\sqrt{L}. \tag{21}$$

The introduced formulation transforms data from an initial condition to the principal orientation, in which variables tend to change in its direction. Figure 2 indicates the initial and oriented data according to the presented contents. It is the novelty of the BHMO which calculates the principal orientation of each variable and the cost function, and directs them into the global best.

## Computational details

According to the mentioned physical simulation and the mathematical kernel, the Black Hole Mechanics Optimization (BHMO) has been developed with the following details.

### Step 1: data generation (star positions)

If the total problem search space is assumed as a space–time, then it is possible to generate initial variables in the feasible domain as star positions. For example, consider the cost function of an assumed problem as:

$$f(x, y, z) = \sin(x) + \cos(y) + \sec(z). \tag{22}$$

It is possible to generate the initial data as the position of the stars according to Eq. (23).

$$\left\{ \begin{array}{l} X = \mathrm{rand}(1, n) \\ Y = \mathrm{rand}(1, n) \\ Z = \mathrm{rand}(1, n) \end{array} \right\}, \tag{23}$$

where $n$ is the number of stars in the space–time (or the number of variables in problem). It is obvious that the current assumed problem is in four-dimensional space with $x$, $y$, $z$, and $f(x, y, z)$ coordinates in which $x$, $y$, and $z$ are the $i$th member of set X, Y, and Z, respectively.

### Step 2: Kerr black hole creation

After locating the positions of the stars (data generation) and their evaluation, the covariance matrix of the initial position of the stars and their costs must be created. Note that each type of variable ($X$, $Y$, and $Z$) must be considered independently with total costs ($f(x, y, z)$) in a two-dimensional space. For instance, for the assumed example, in this step, COV($X$, $f(x, y, z)$), COV($Y$, $f(x, y, z)$), and COV($Z$, $f(x, y, z)$) must be calculated. After that, according to the mentioned transformation in "Mathematical kernel", the transformed vector $X$, $Y$, $Z$ should be calculated. Then, the initial data is transformed around a central point, which can be considered as the Kerr black hole position.

As explained previously, a Kerr black hole is the one which possesses only mass ($M$) and angular momentum ($J$) without any electrical charge ($Q$). Hence, it rotates around a central axis. Also, its adjacent stars circulate due to its

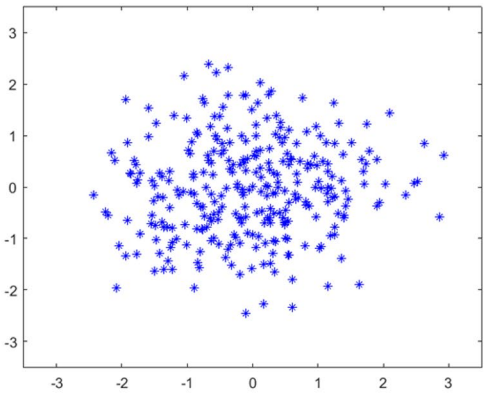


**a** The initial data in the search space of the problem.

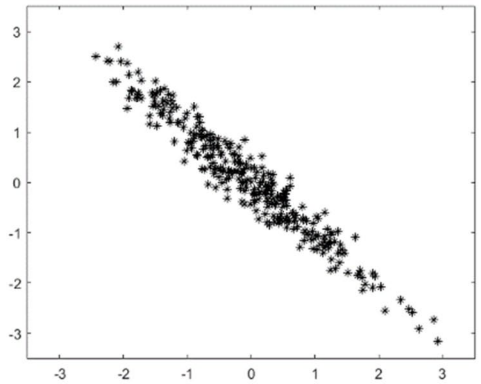


**b** The orientated data and principal directions found by using covariance matrix transformation.

**Fig. 2** **a** The initial data in the search space of the problem, **b** the orientated data and principal directions found by using covariance matrix transformation

gravity. If the variance of variables (subjected to the Kerr black hole position) is assumed as its entropy, then the area of the event horizon can be calculated using the Bekenstein–Hawking equation (Eq. 2). Therefore, the parameter $a$ can be obtained using Eq. (7). By considering minimum eigenvalues of each covariance matrix as feasible radiuses, it is possible to assume the mass of the Kerr black hole as the number of its contiguous stars in their feasible radiuses. In the following, the parameter $r$ must be obtained by Eq. (6). Finally, the speed of each star can be calculated using Eq. (12).

### Step 3: Schwarzschild black hole creation

The Kerr black hole gravity makes a circular gravity field which forces the stars to move around a circular axis and close to its center. This procedure provides the exploration of the algorithm. In another word, the stars due to Kerr black hole gravity explore all the feasible space–time (problem search space). However, it is obligatory to define another sub-space–time (sub-search space) in the vicinity of the surmised global best. The minimum value after covariance transformation is the most probable position of the global best. Therefore, new data must be generated in its vicinity.

In the Schwarzschild black hole, angular momentum ($J$) and electrical charge ($Q$) are equal to zero, and it contains only the mass ($M$). If the minimum eigenvalue of each covariance matrix is assumed as the feasible radius in each direction, then it is possible to define parameter $r$ for Schwarzschild black hole as a vector addition of feasible radiuses. After that, the total mass ($M$) of Schwarzschild black hole can be calculated using Eq. (6). Now, new data must be generated equal to the calculated mass in the vicinity of its radius.

Therefore, the Schwarzschild black hole controls the exploitation of the algorithm and generates new data in each step in the vicinity of the probable position of the global best. The specific exploration and exploitation of the BHMO

algorithm make it more efficient and faster than the other methods. This efficiency is shown through various examples in "Examples".

### Step 4: data elimination

The newly generated data in the previous step must be evaluated in this step. Finally, the distant stars based on elite selection procedures such as roulette wheel selection (RWS) will be eliminated.

$$f(x, y) = 3\sin(x) + 5\cos(y). \tag{24}$$

This trigonometry problem contains many local minima and some global best. The BHMO can find all global bests in only 15 iterations and 0.04 s (using a Lenovo IdeaPad 500 Laptop), as illustrated in Figs. 3 and 4. Also, at the end of the process, there are a few near-global stars conducted by BHMO.

In the following the pseudo code of the Black Hole Mechanics Optimization is presented as Algorithm 1.

**Algorithm 1** Pseudo-code of the BHMO algorithm

**Inputs:** The population size *ns*, and the maximum number of iterations *it*

**Outputs:** The position of global best and its objective value.

**Initialization:** Initialize the random stars in the galaxy (search space)

Calculate the objective values of the stars

Create covariance matrix of the design variables and their objective value

Detect the position of the kerr black hole

Update position of the stars

Detect the position of the Schwarzschild black hole

Impose the circular field to the position of stars

Eliminate distant stars from the galaxy (search space)

**Main Loop: while** (terminating condition is not met) do

Calculate the objective values of the stars

Create covariance matrix of the design variables and their objective value

Detect the position of the kerr black hole

Update position of the stars

Detect the position of the Schwarzschild black hole

Impose the circular field to the position of stars

Eliminate distant stars from the galaxy (search space)

**end**

**Return** $\text{Star}_{\text{optimal}}$

### The results of an example

By conducting the data using mathematical kernel and physical simulation, the algorithm must find the global best very fast as well as not get trapped in local optimums. A three-dimensional problem can be defined as:

## Examples

In this section, the BHMO algorithm is employed to solve broad types of problems. The problems are divided into two categories. "Benchmark optimization problems" contain some mathematical problems which are usually considered

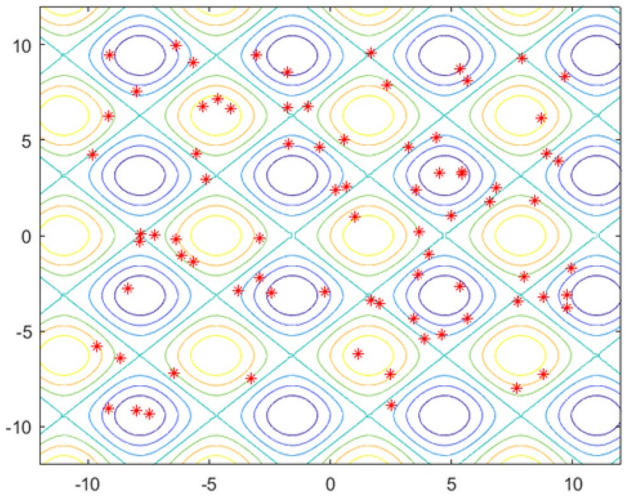


**Fig. 3** The efforts of BHMO in problem "The results of an example" (Iteration 1)

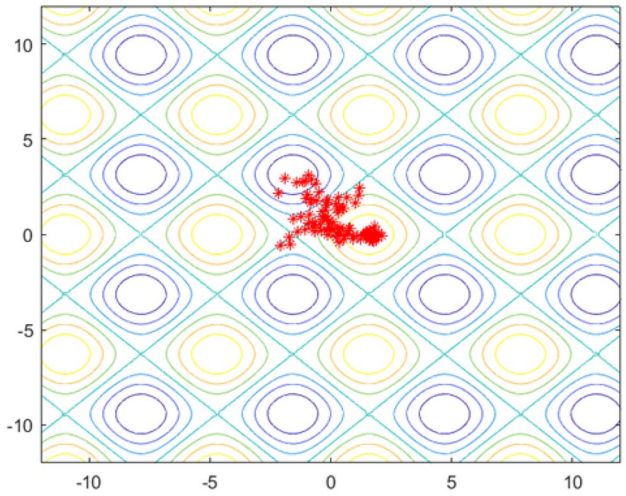


**Fig. 4** The efforts of BHMO in problem "The results of an example" (Iteration 15)

as benchmark optimization problems. The last category is dedicated to some structural engineering problems which are real-size structures with real-loading conditions.

## Benchmark optimization problems

To verify the proposed method, it seems appropriate to study some mathematical benchmark problems in which the optimum solution is analytically available. Table 2 contains some test functions, their names, optimum solution, and domains (Chen et al. 2013).

As mentioned before, the total cost of an algorithm can be defined as the consumed time and working memory. Therefore, to assay the efficiency of the new proposed algorithm, it is essential to compare its total cost with the other well-known algorithms. Table 3 contains the memory cost of the GA, PSO, CBO, and Black Hole Mechanics Optimization (BHMO) for test functions 1–9.

The relative diagrams of each problem for the BHMO algorithm are shown in Figs. 5, 6, 7, 8, 9, 10, 11, 12 and 13.

Also, Table 4 contains the details of each problem.

In the following, the consumed times of each algorithm for solving problems 1–17, which are more complicated, are compared in Table 5.

As illustrated in Tables 2, 3, 4 and 5, the Black Hole Mechanics Optimization is more efficient and economical than others. This efficiency is due to the mathematical kernel, which detects the optimum direction to conduct variables in each step. This navigated conducting leads to an impressive decrease in the total algorithm iterations, which is equal to the convergence speed. Moreover, the appropriate physical stimulation leads to the correct updating of variables in the vicinity of the global best. i.e., the best cost is found faster and more accurately. In other words, both the exploration and exploitation procedures improved computationally using the proposed mathematical kernel and physical simulation.

## Structural engineering examples

The potency of the proposed algorithm has been examined previously. In this section, the applicability of BHMO is investigated by solving more complicated structural engineering examples. The following examples, which are real-size structures with real-loading conditions are optimized by BHMO and other well-known and efficient algorithms subjected to various constraints. Finally, the results are compared together, and outcomes are reported.

### Truss problems

The stress constraints for truss problems are enforced according to ASD-AISC (AISC 1989) design code provisions.

$$\begin{cases} \sigma_i^+ = 0.6F_y & \text{for } \sigma_i \geq 0 \\ \sigma_i^- & \text{for } \sigma_i < 0 \end{cases}, \tag{25}$$

where $F_y$ is the yield strength and $\sigma_i^-$ is calculated depending on the elastic and inelastic buckling of the members.

$$\sigma_i^- = \begin{cases} \left[\left(1 - \dfrac{\lambda_i^2}{2C_c^2}\right)F_y\right] \Big/ \left[\dfrac{5}{3} + \dfrac{3\lambda_i}{8C_c} - \dfrac{\lambda_i^3}{8C_c^3}\right] & \text{for } \lambda_i < C_c \\ \dfrac{12\pi^2 E}{23\lambda_i^2} & \text{for } \lambda_i \geq C_c \end{cases}, \tag{26}$$

**Table 2** The test functions (benchmark problems) information

| Test function | Name | Domain | Optimum |
|---|---|---|---|
| $f_1(x) = \sum_{i=1}^{n} x_i^2$ | Sphere | $[-100, 100]$ | 0 |
| $f_2(x) = \sum_{i=1}^{n} \lvert x_i \rvert + \prod_{i=1}^{n} \lvert x_i \rvert f_3(x) = \sum_{i=1}^{n} \left( \sum_{j=1}^{i} x_j \right)^2$ | Schwefel's P2.22 | $[-10, 10]$ | 0 |
| $f_3(x) = \sum_{i=1}^{n} \left( \sum_{j=1}^{i} x_j \right)^2$ | Quadric | $[-100, 100]$ | 0 |
| $f_4(x) = \sum_{i=1}^{n-1} [100(x_{i+1} - x_i^2)^2 + (x_i - 1)^2]$ | Rosenbrock's | $[-10, 10]$ | 0 |
| $f_5(x) = \sum_{i=1}^{n} (\lfloor x_i + 0.5 \rfloor)^2$ | Step | $[-100, 100]$ | 0 |
| $f_6(x) = \sum_{i=1}^{n} [x_i^2 - 10\cos(2\pi x_i) + 10]$ | Rastrigin | $[-5.12, 5.12]$ | 0 |
| $f_7(x) = \sum_{i=1}^{n} [y_i^2 - 10\cos(2\pi y_i) + 10]$[a] | Noncontinuous Rastrigin | $[-5.12, 5.12]$ | 0 |
| $f_8(x) = -20e^{(-0.2\sqrt{\frac{1}{n}\sum_{i=1}^{n} x_i^2})} - e^{(\frac{1}{n}\sum_{i=1}^{n} \cos 2\pi x_i)} + e + 20$ | Ackley | $[-32, 32]$ | 0 |
| $f_9(x) = \frac{1}{4000}\sum_{i=1}^{n} x_i^2 - \prod_{i=1}^{n} \cos(\frac{x_i}{\sqrt{i}}) + 1$ | Griewank | $[-600, 600]$ | 0 |
| $f_{10}(x) = \sum_{i=1}^{n} -x_i \sin(\sqrt{\lvert x_i \rvert})$ | Schwefel's | $[-500, 500]$ | −12,569.5 |
| $f_{11}(x) = \frac{\pi}{n}\{1 - \sin^2(\pi y_1) + \sum_{i=1}^{n-1} (y_i - 1)^2[1 + 10\sin^2(\pi y_{i+1})])$ $+(y_n - 1)^2\} + \sum_{i=1}^{n} u(x_i, 10, 100, 4), y_i = 1 + 0.25(x_i + 1)$ [b] | Generalized Penalized | $[-50, 50]$ | 0 |
| $f_{12}(x) = \frac{1}{10}\{10\sin^2(3\pi x_1) + \sum_{i=1}^{n-1} (x_i - 1)^2[1 + \sin^2(3\pi x_{i+1})]$ | Generalized Penalized | $[-50, 50]$ | 0 |
| $f_{13}(x) = \sum_{i=1}^{n} (\sum_{j=1}^{i} z_j)^2 - 450, z = x - o$[c] | Shifted Schwefel's P1.2 | $[-100, 100]$ | −450 |
| $f_{14}(x) = \sum_{i=1}^{n} (10^6)^{\frac{i-1}{n-1}} z_i^2 - 450,\ z = (x - o) \times M$[c] | Shifted Rotated High Conditioned Elliptic | $[-100, 100]$ | −450 |
| $f_{15}(x) = \sum_{i=1}^{n-1} [100(z_{i+1} - z_i^2)^2 + (z_i - 1)^2] + 390, z = x - o + 1$[c] | Shifted Rosenbrock's | $[-100, 100]$ | 390 |
| $f_{16}(x) = \sum_{i=1}^{n} [z_i^2 - 10\cos(2\pi z_i) + 10] - 330, z = (x - o) \times M$[c] | Shifted Rotated Rastrigin's | $[-5, 5]$ | -330 |
| $f_{17}(x) = \sum_{i=1}^{n} (\sum_{k=0}^{k_{\max}} [a^k \cos(2\pi b^k(z_i + 0.5))])$ $-n\sum_{k=0}^{k_{\max}} [a^k \cos(2\pi b^k \cdot 0.5)] + 90,$ $a = 0.5, b = 3, k_{\max} = 20, z = (x - o) \times M$ [c] | Shifted Rotated Weierstrass | $[-0.5, 0.5]$ | 90 |

[a] In $f_7, y_i = \left\{ \begin{array}{ll} x_i, & \lvert x_i \rvert \geq 0.5 \\ \frac{\text{round}(2x_i)}{2}, & \lvert x_i \rvert \geq 0.5 \end{array} \right\}$.

[b] In $f_{11}$ and $f_{12} u(x_j, a, k, m) = \left\{ \begin{array}{ll} k(x_j - a)^m & x_j > a \\ 0 & -a \leq x_j \leq a \\ k(-x_j - 1)^m & x_j < -a \end{array} \right\}$.

[c] In $f_{13-17}$, $\boldsymbol{o}$ is a shifted vector, and $\boldsymbol{M}$ is a transformation matrix. Please refer to (Chen et al. 2013; Suganthan et al. 2005).

where $E$, $\lambda_i$ and $C_c$ are the modulus of elasticity, the slenderness ratio, and the parameter that divides the elastic and inelastic buckling regions, respectively.

$$C_c = \sqrt{\frac{2\pi^2 E}{F_y}}, \tag{27}$$

$$\lambda_i = \frac{kl_i}{r_i}, \tag{28}$$

where $k$ is the effective length factor, which is set equal to 1 for all truss members, $l_i$ is the member length, and $r_i$ is the minimum radius of gyration.

The maximum slenderness ratio is limited to 300 for tension members, and it is recommended to be 200 for compression members.

**Optimum design of a 72-bar 3D-truss** For the schematic of a 3D-truss structure containing 72 bars shown in Fig. 14, Young's modulus and the material density are 107 psi (68.95 GPa) and 0.1 lb/in$^3$ (2767.990 kg/m$^3$), respectively. Two independent loading cases are applied to the truss, which are listed in Table 6. The maximum stress developed in the elements must be less than ± 25 ksi (± 172.375 MPa). The nodes are subjected to the displacement limits of ± 0.25 in (± 6.35 mm). Due to structural symmetry, the elements

**Table 3** The memory cost of the GA, PSO, CBO, and BHMO for problems 1–9

| Problem number | Genetic Algorithm | | | PSO | | | CBO | | | BHMO | | |
|---|---|---|---|---|---|---|---|---|---|---|---|---|
| | NFE | Variables | Best Cost | NFE | Variables | Best Cost | NFE | Variables | Best Cost | NFE | Variables | Best Cost[a] |
| 1 | 200 | 300 | 0 | 120 | 60 | 0 | 90 | 60 | 0 | 10 | 60 | 0 |
| 2 | 200 | 300 | 0 | 120 | 60 | 0 | 90 | 60 | 0 | 10 | 60 | 0 |
| 3 | 200 | 300 | 0 | 120 | 60 | 0 | 90 | 60 | 0 | 10 | 60 | 0 |
| 4 | 200 | 300 | 0 | 120 | 60 | 0 | 90 | 60 | 0 | 10 | 60 | 0 |
| 5 | 200 | 300 | 0 | 120 | 60 | 0 | 90 | 60 | 0 | 10 | 60 | 0 |
| 6 | 200 | 300 | 0 | 120 | 60 | 0 | 90 | 60 | 0 | 10 | 60 | 0 |
| 7 | 200 | 300 | 0 | 120 | 60 | 0 | 90 | 60 | 0 | 10 | 60 | 0 |
| 8 | 200 | 300 | 0 | 120 | 60 | 0 | 90 | 60 | 0 | 10 | 60 | 0 |
| 9 | 250 | 500 | 0 | 150 | 80 | 0 | 110 | 60 | 0 | 30 | 60 | 0 |

[a]The results of the BHMO algorithm are calculated as the average of the final results of 40 times different runs

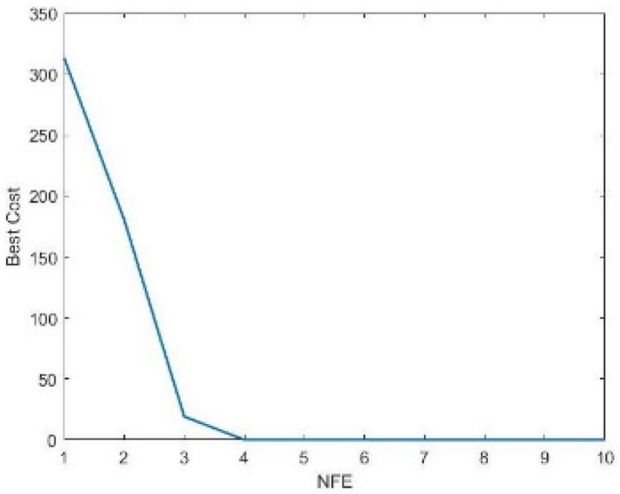


**Fig. 5** Relative diagrams of the BHMO algorithm effort in problem 1

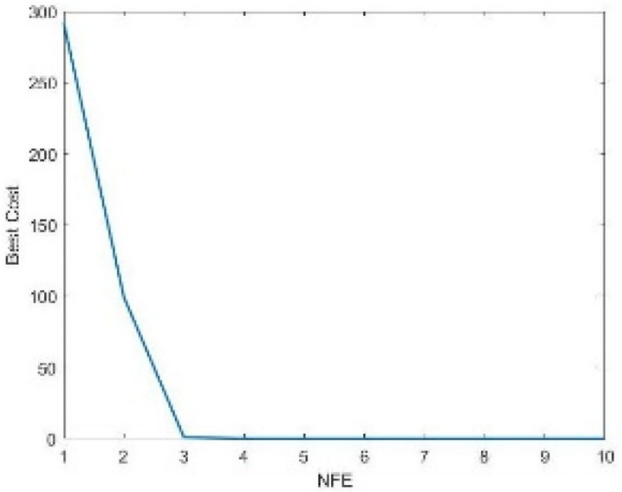


**Fig. 7** Relative diagrams of the BHMO algorithm effort in problem 3

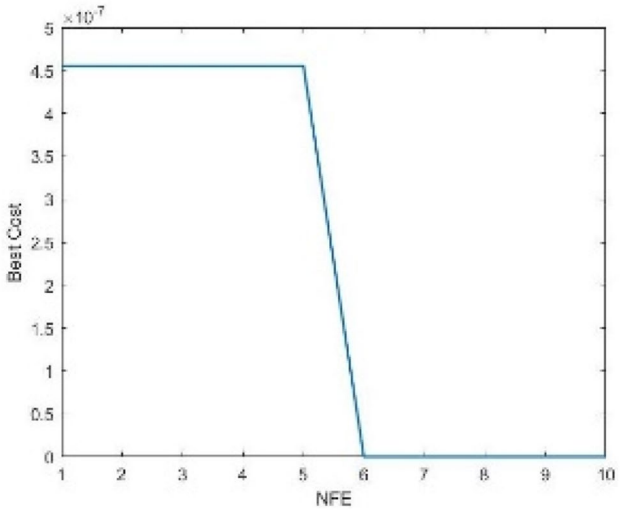


**Fig. 6** Relative diagrams of the BHMO algorithm effort in problem 2

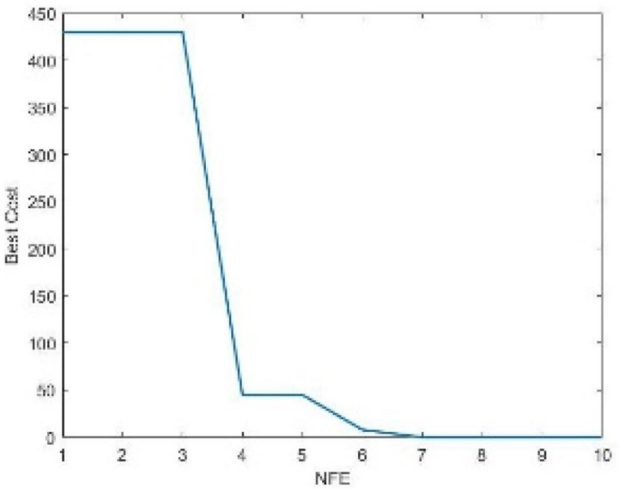


**Fig. 8** Relative diagrams of the BHMO algorithm effort in problem 4

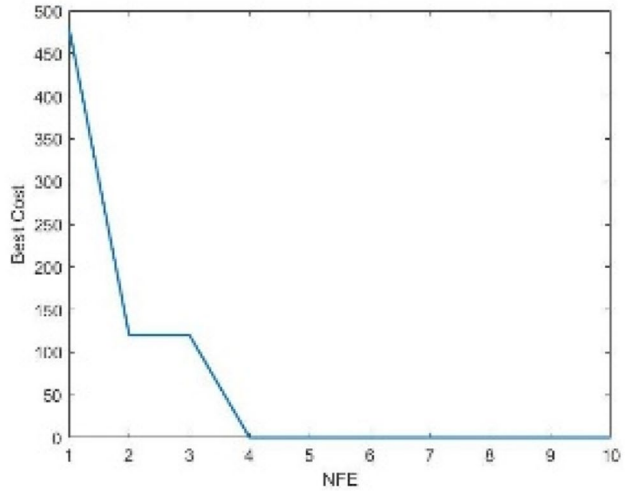


**Fig. 9** Relative diagrams of the BHMO algorithm effort in problem 5

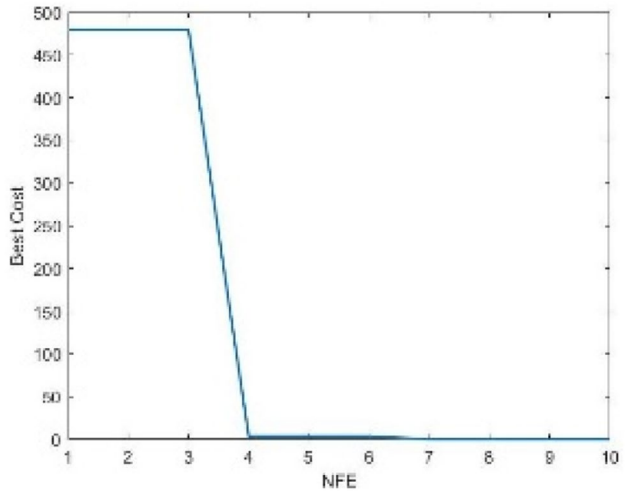


**Fig. 10** Relative diagrams of the BHMO algorithm effort in problem 6

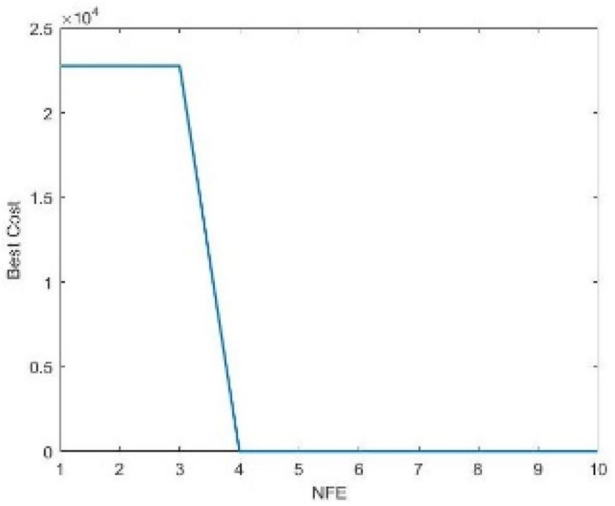


**Fig. 11** Relative diagrams of the BHMO algorithm effort in problem 7

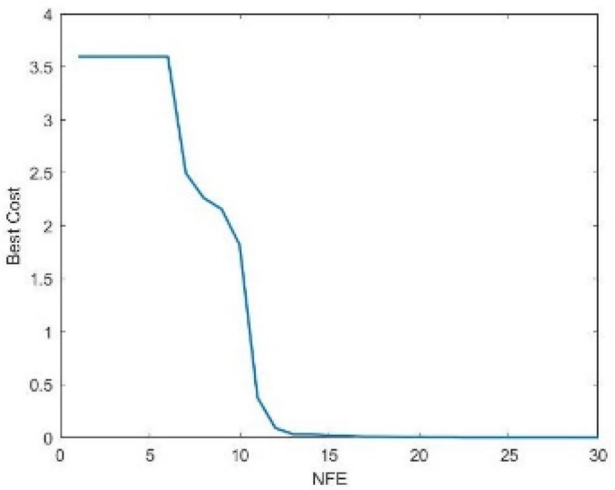


**Fig. 12** Relative diagrams of the BHMO algorithm effort in problem 8

are classified into 16 groups: (1) A1–A4, (2) A5–A12, (3) A13– A16, (4) A17–A18, (5) A19–A22, (6) A23–A30, (7) A31–A34, (8) A35–A36, (9) A37–A40, (10) A41–A48, (11) A49–A52, (12) A53–A54, (13) A55–A58, (14) A59–A66 (15), A67–A70, and (16) A71–A72. Also, in the selection process of cross-sectional area, a list of 64 discrete sections from 0.111 to 33.5 $in^2$ (71.613–21,612.860 $mm^2$) is used (Kaveh and Talatahari 2010b). The final calculated results are listed in Table 7.

**Optimum design of the 582-bar 3D-tower** Figure 15 schematizes a 3D-tower truss with 582 bars. Considering the structural symmetry about the x- and y-directions, the 582 members are divided into 32 groups. A single load case is considered: lateral loads of 1.12 kips (5.0 kN) is applied in both the x- and y-directions and a vertical load of − 6.74 kips (− 30 kN) is applied in the z-direction at all nodes of the tower. A set of W-shaped standard steel sections based on area and radii of gyration properties is utilized in the size optimization of the truss. The lower and upper bounds on this variable are taken as 6.16 and 215 $in^2$ (i.e., 39.74 and 1387.09 $cm^2$). Also, the maximum nodal displacements in all coordinate directions are limited to ±3.15 in (i.e., ±8 cm). The corresponding results are reported in Tables 8 and 9.

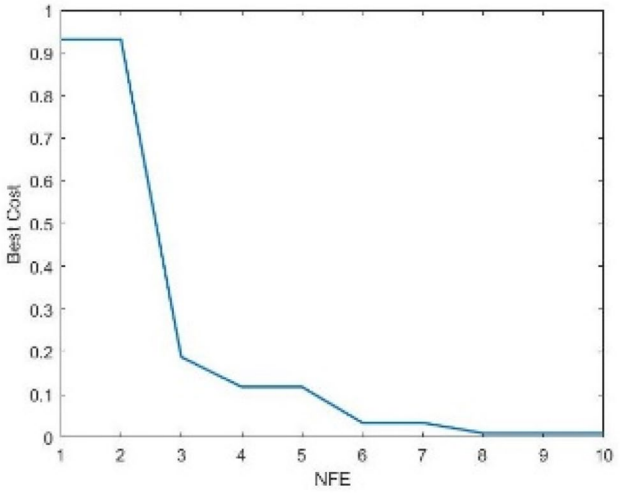


**Fig. 13** Relative diagrams of the BHMO algorithm effort in problem 9

### Steel frame problems

Constraint conditions for steel frames are imposed according to the LRFD-AISC provisions (AISC 2001).

1. Maximum lateral displacement

$$\frac{\Delta_T}{H} - R \leq 0, \tag{29}$$

where $\Delta_T$ is the maximum lateral displacement, $H$ is the height of the frame structure, and $R$ is the maximum drift index which is equal to $1/300$.

2. The inter-story displacements constraints

$$\frac{d_i}{h_i} - R_i \leq 0,\ i = 1, 2, ..., \text{ns}, \tag{30}$$

**Table 4** Details of the BHMO process for problems 1–9

| Problem number | Analytical optimum | Best star position cost[a] | Relative error (%) | Iteration | Total time (s)[b] |
|---|---|---|---|---|---|
| 1 | 0 | $2.52E-09$ | 0 | 10 | 1.92 |
| 2 | 0 | $3.21E-25$ | 0 | 10 | 2.34 |
| 3 | 0 | $5.78E-48$ | 0 | 10 | 2.32 |
| 4 | 0 | 0 | 0 | 10 | 2.67 |
| 5 | 0 | 0 | 0 | 10 | 2.21 |
| 6 | 0 | $8.25E-09$ | 0 | 10 | 2.76 |
| 7 | 0 | $6.21E-11$ | 0 | 10 | 2.31 |
| 8 | 0 | $7.42E-05$ | 0 | 10 | 2.63 |
| 9 | 0 | $2.62E-05$ | 0 | 30 | 2.67 |

[a]The results of the BHMO algorithm are calculated as the average of the final results of 40 times different runs

[b]The consumed time is reported as the sum of all runs of the algorithm

**Table 5** Consumed time of GA, PSO, CBO, and BHMO in problems 10–17

| Problem number | Genetic algorithm | | | PSO | | | CBO | | | BHMO | | |
|---|---|---|---|---|---|---|---|---|---|---|---|---|
| | NFE | Time | Best cost | NFE | Time | Best cost | NFE | Time | Best cost | NFE | Time | Best cost |
| 10 | 100 | 129.2 | −3057.314 | 100 | 43.6 | −8220.147 | 100 | 21.3 | −11,534.523 | 100 | 0.82 | −12,569.495 |
| 11 | 100 | 122.3 | 139.27 | 100 | 45.1 | 0 | 100 | 20.7 | 0 | 100 | 0.86 | 0 |
| 12 | 100 | 122.6 | 80.612 | 100 | 44.7 | 5.286 | 100 | 22.4 | 0 | 100 | 0.83 | 0 |
| 13 | 100 | 140.3 | 12.356 | 100 | 49.2 | −450 | 100 | 28.6 | −450 | 100 | 1.29 | −450 |
| 14 | 100 | 146.9 | −80.36 | 100 | 50.8 | −410.32 | 100 | 30.7 | −450 | 100 | 1.31 | −450 |
| 15 | 100 | 164.3 | 533.25 | 100 | 52.6 | 390 | 100 | 32.4 | 390 | 100 | 1.84 | 390 |
| 16 | 100 | 184.7 | 1.835 | 100 | 60.1 | −256.34 | 100 | 38.3 | −103.62 | 100 | 2.23 | −330 |
| 17 | 100 | 190.6 | 503.14 | 100 | 63.0 | 259.42 | 100 | 41.2 | 284.36 | 100 | 2.31 | 90 |

[a]The number of variables for each algorithm is constant and equal to 60

[b]The results of consumed time are reported in seconds

[c]The results of the BHMO algorithm are calculated as the average of the final results of 40 times different runs

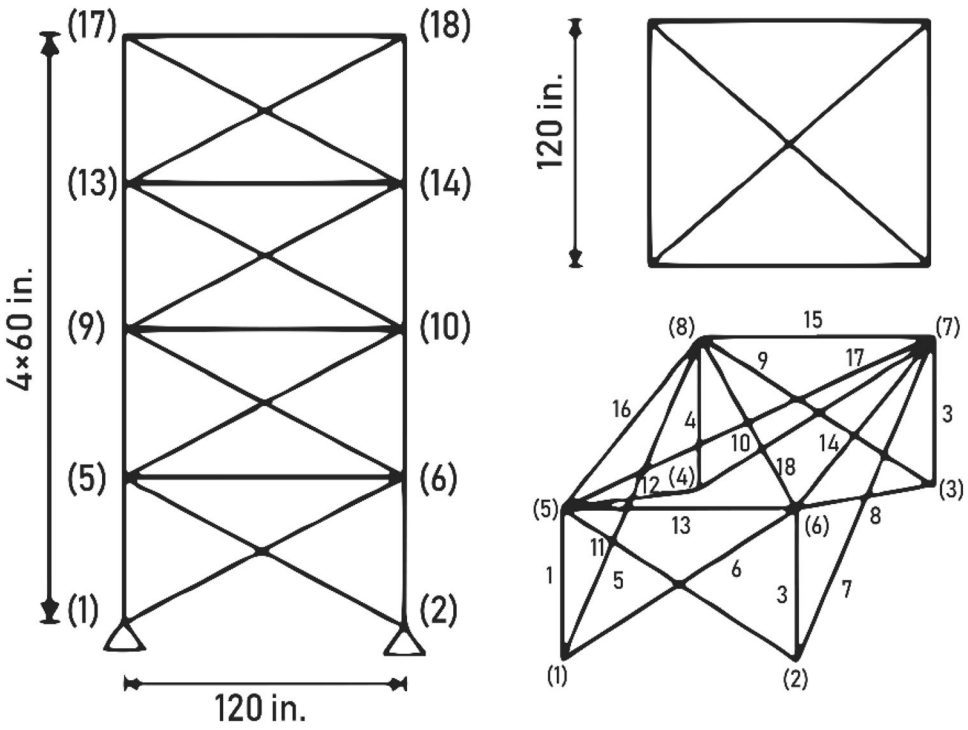


**Fig. 14** Schematic of a 72-bar 3D-truss structure

where $d_i$ is the inter-story drift, $h_i$ is the story height of the $i$th floor, $ns$ is the total number of stories, and $R_i$ is the inter-story drift index (1/300).

3. The strength constraints

$$\begin{cases} \dfrac{P_u}{2\varphi_c P_n} + \dfrac{M_u}{\varphi_b M_n} - 1 \le 0, & \text{for } \dfrac{P_u}{\varphi_c P_n} < 0.2 \\ \dfrac{P_u}{\varphi_c P_n} + \dfrac{8M_u}{9\varphi_b M_n} - 1 \le 0, & \text{for } \dfrac{P_u}{\varphi_c P_n} \ge 0.2 \end{cases}, \tag{31}$$

where $P_u$ is the required strength (tension or compression), $P_n$ is the nominal axial strength (tension or compression), $\varphi_c$ is the resistance factor, $M_u$ is the required flexural strength, $M_n$ is the nominal flexural strength, and $\varphi_b$ denotes the flexural resistance reduction factor.

$$\begin{cases} \varphi_c = 0.9 & \text{for tension} \\ \varphi_c = 0.85 & \text{for compression} \end{cases}, \tag{32}$$

$$\varphi_b = 0.9, \tag{33}$$

$$\begin{cases} P_n = A_g F_y & \text{for tension} \\ P_n = A_g F_{cr} & \text{for compression} \end{cases}, \tag{34}$$

where $A_g$ is the cross-sectional area of a member, and $F_{cr}$ can be computed as in Eq. (35).

$$\begin{cases} F_{cr} = (0.658^{\lambda_c^2})F_y, & \text{for } \lambda_c \le 1.5 \\ F_{cr} = (\dfrac{0.877}{\lambda_c^2})F_y, & \text{for } \lambda_c > 1.5 \end{cases}, \tag{35}$$

$$\lambda_c = \frac{kl}{r\pi}\sqrt{\frac{F_y}{E}}, \tag{36}$$

where $k$ is the effective length factor that is calculated by (Dumonteil 1992):

**Table 6** Loading conditions for the 72-bar 3D-truss

| Node | First condition | | | Second condition | | |
|---|---|---|---|---|---|---|
| | $F_x$ (kips) | $F_y$ (kips) | $F_z$ (kips) | $F_x$ (kips) | $F_y$ (kips) | $F_z$ (kips) |
| 17 | 0 | 0 | −5.0 | −5.0 | −5.0 | −5.0 |
| 18 | 0 | 0 | −5.0 | 0 | 0 | 0 |
| 19 | 0 | 0 | −5.0 | 0 | 0 | 0 |
| 20 | 0 | 0 | −5.0 | 0 | 0 | 0 |

**Table 7** Comparison of the optimized design of the 72-bar 3D-truss structure obtained by different algorithms

| Element type | Members | Area of cross sections ($in^2$) | | | |
|---|---|---|---|---|---|
| | | VPS (Kaveh and Ilchi 2016) | CBO (Kaveh and Ilchi 2016) | TLBO | BHMO |
| 1 | 1–4 | 2.1 | 2.1 | 2 | 1.8 |
| 2 | 5–12 | 0.7 | 0.6 | 0.6 | 0.4 |
| 3 | 13–16 | 0.2 | 0.1 | 0.1 | 0.1 |
| 4 | 17–18 | 0.2 | 0.1 | 0.1 | 0.1 |
| 5 | 19–22 | 1.4 | 1.2 | 1.1 | 1.2 |
| 6 | 23–30 | 0.7 | 0.4 | 0.4 | 0.4 |
| 7 | 31–34 | 0.2 | 0.1 | 0.1 | 0.1 |
| 8 | 35–36 | 0.2 | 0.1 | 0.1 | 0.1 |
| 9 | 37–40 | 0.7 | 0.4 | 0.6 | 0.4 |
| 10 | 41–48 | 0.7 | 0.6 | 0.6 | 0.4 |
| 11 | 49–52 | 0.2 | 0.1 | 0.1 | 0.1 |
| 12 | 53–54 | 0.2 | 0.1 | 0.1 | 0.1 |
| 13 | 55–58 | 0.2 | 0.2 | 0.1 | 0.2 |
| 14 | 59–66 | 0.7 | 0.6 | 0.6 | 0.6 |
| 15 | 67–70 | 0.7 | 0.4 | 0.4 | 0.3 |
| 16 | 71–72 | 0.7 | 0.7 | 0.6 | 0.6 |
| Total weight (lb) | | 499.8 | 392.7 | 387.6 | 351.9 |

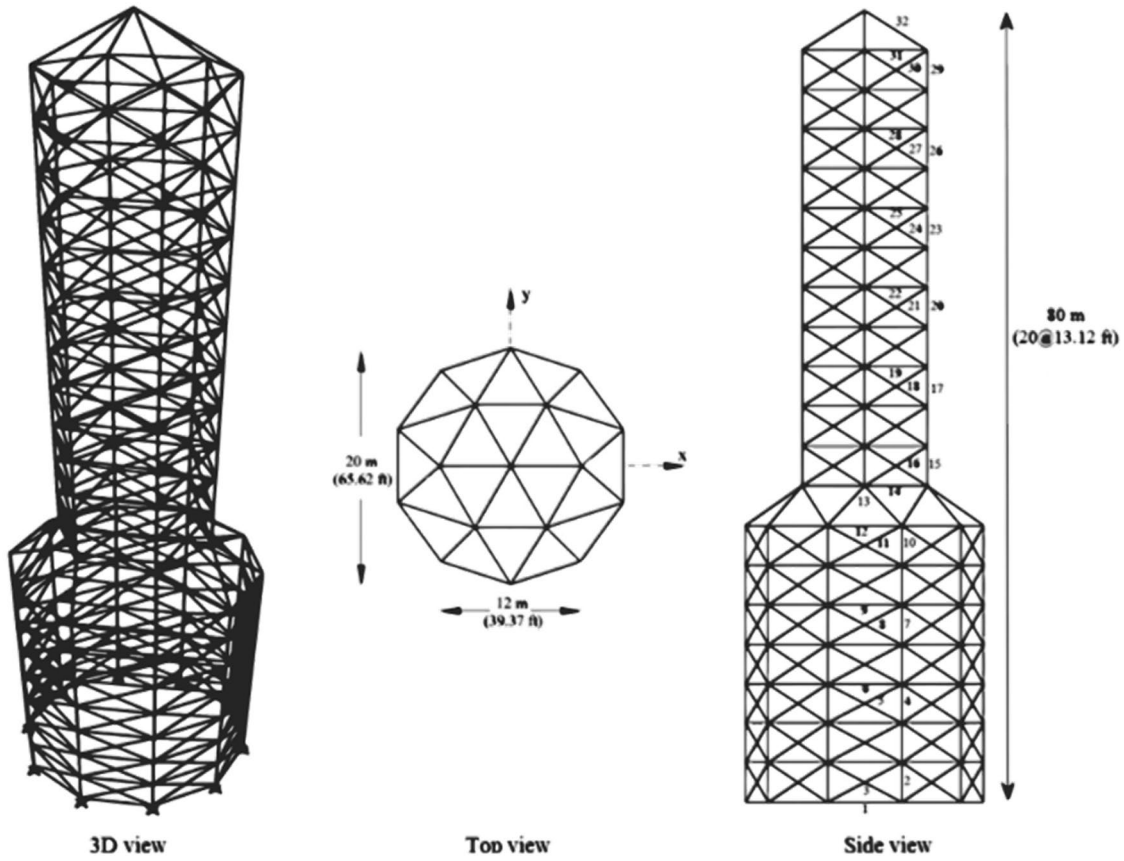


**Fig. 15** Schematic of a 582-bar 3D-tower

**Table 8** Comparison of the optimized design of the 582-bar 3D-tower obtained by different algorithms

| Element type* | Area of cross sections ($in^2$) | | | |
|---|---|---|---|---|
| | VPS (Kaveh and Ilchi 2016) | CBO (Kaveh and Ilchi 2016) | TLBO | BHMO |
| 1 | 6.2 | 7.1 | 6.2 | 6.2 |
| 2 | 23.2 | 20.1 | 24.1 | 24.1 |
| 3 | 7.1 | 8.3 | 8.3 | 7.1 |
| 4 | 17.6 | 17.6 | 14.7 | 14.7 |
| 5 | 7.1 | 7.1 | 7.1 | 7.1 |
| 6 | 6.2 | 7.1 | 6.2 | 6.2 |
| 7 | 14.1 | 14.7 | 15.6 | 14.1 |
| 8 | 7.1 | 7.1 | 7.7 | 7.1 |
| 9 | 6.2 | 7.6 | 6.2 | 6.2 |
| 10 | 13.3 | 11.2 | 14.1 | 14.4 |
| 11 | 7.1 | 8.8 | 7.1 | 7.1 |
| 12 | 20.0 | 21.1 | 17.9 | 17.9 |
| 13 | 21.8 | 21.5 | 24.1 | 22.3 |
| 14 | 14.1 | 15.6 | 14.7 | 14.4 |
| 15 | 22.3 | 25.3 | 21.8 | 21.8 |
| 16 | 9.1 | 9.1 | 11.7 | 9.1 |
| 17 | 6.2 | 17.6 | 15.6 | 15.6 |
| 18 | 19.7 | 7.1 | 7.3 | 7.1 |
| 19 | 7.1 | 10.6 | 6.2 | 6.2 |
| 20 | 6.2 | 11.5 | 11.7 | 10.0 |
| 21 | 11.7 | 7.1 | 7.1 | 7.1 |
| 22 | 7.1 | 7.1 | 6.2 | 6.2 |
| 23 | 6.2 | 9.1 | 7.7 | 6.2 |
| 24 | 6.5 | 8.3 | 7.7 | 7.1 |
| 25 | 7.1 | 6.2 | 6.5 | 6.2 |
| 26 | 6.2 | 7.1 | 6.5 | 6.5 |
| 27 | 6.2 | 8.3 | 7.3 | 7.1 |
| 28 | 7.1 | 6.49 | 6.2 | 6.2 |
| 29 | 11.7 | 7.1 | 6.2 | 6.2 |
| 30 | 6.2 | 7.1 | 7.1 | 7.1 |
| 31 | 7.1 | 6.49 | 6.2 | 6.2 |
| 32 | 7.1 | 7.1 | 7.3 | 7.1 |
| Total weight (lb) | 372,514 | 385,623 | 370,718 | 356,801 |

**Table 9** Comparison of the optimized design of the 582-bar 3D-tower obtained by different algorithms

| Element type* | Type of cross sections | | | |
|---|---|---|---|---|
| | VPS (Kaveh and Ilchi 2016) | CBO (Kaveh and Ilchi 2016) | TLBO | BHMO |
| 1 | W 8×21 | W 8×24 | W 8×21 | W 8×21 |
| 2 | W 12×79 | W 24×68 | W 14×82 | W 14×82 |
| 3 | W 8×24 | W 8×28 | W 8×28 | W 8×24 |
| 4 | W 18×60 | W 18×60 | W 21×50 | W 21×50 |
| 5 | W 8×24 | W 8×24 | W 8×24 | W 8×24 |
| 6 | W 8×21 | W 8×24 | W 8×21 | W 8×21 |
| 7 | W 14×48 | W 21×50 | W 14×53 | W 14×48 |
| 8 | W 8×24 | W 8×24 | W 12×26 | W 8×24 |
| 9 | W 8×21 | W 10×26 | W 8×21 | W 8×21 |
| 10 | W 16×45 | W 14×38 | W 14×48 | W 10×49 |
| 11 | W 8×24 | W 12×30 | W 8×24 | W 8×24 |
| 12 | W 21×68 | W 12×72 | W 14×61 | W 14×61 |
| 13 | W 14×74 | W 21×73 | W 14×82 | W 18×76 |
| 14 | W 14×48 | W 14×53 | W 21×50 | W 10×49 |
| 15 | W 18×76 | W 18×86 | W 14×74 | W 14×74 |
| 16 | W 8×31 | W 8×31 | W 8×40 | W 8×31 |
| 17 | W 8×21 | W 18×60 | W 14×53 | W 14×53 |
| 18 | W 16×67 | W 8×24 | W 6×25 | W 8×24 |
| 19 | W 8×24 | W 16×36 | W 8×21 | W 8×21 |
| 20 | W 8×21 | W 10×39 | W 8×40 | W 14×34 |
| 21 | W 8×40 | W 8×24 | W 8×24 | W 8×24 |
| 22 | W 8×24 | W 8×24 | W 8×21 | W 8×21 |
| 23 | W 8×21 | W 8×31 | W 12×26 | W 8×21 |
| 24 | W 12×22 | W 8×28 | W 12×26 | W 8×24 |
| 25 | W 8×24 | W 8×21 | W 12×22 | W 8×21 |
| 26 | W 8×21 | W 8×24 | W 12×22 | W 12×22 |
| 27 | W 8×21 | W 8×28 | W 6×25 | W 8×24 |
| 28 | W 8×24 | W 14×22 | W 8×21 | W 8×21 |
| 29 | W 8×40 | W 8×24 | W 8×21 | W 8×21 |
| 30 | W 8×21 | W 8×24 | W 8×24 | W 8×24 |
| 31 | W 8×24 | W 14×22 | W 8×21 | W 8×21 |
| 32 | W 8×24 | W 8×24 | W 6×25 | W 8×24 |

$$k = \sqrt{\frac{1.6G_AG_B + 4.0(G_A + G_B) + 7.5}{G_A + G_B + 7.5}}, \tag{37}$$

where $G_A$ and $G_B$ are stiffness ratios of columns and girders at two end joints, $A$ nd $B$, of the column section being considered, respectively.

**Optimum design of 3-bay 15-story frame structure** The first design example deals with a three-bay 15-story frame, for which the applied loads and the numbering of member groups are shown in Fig. 16. The sway of the top story is limited to 9.25 in (23.5 cm). The material has elastic modulus equal to 29 Msi (200 GPa) and yield stress of 36 ksi

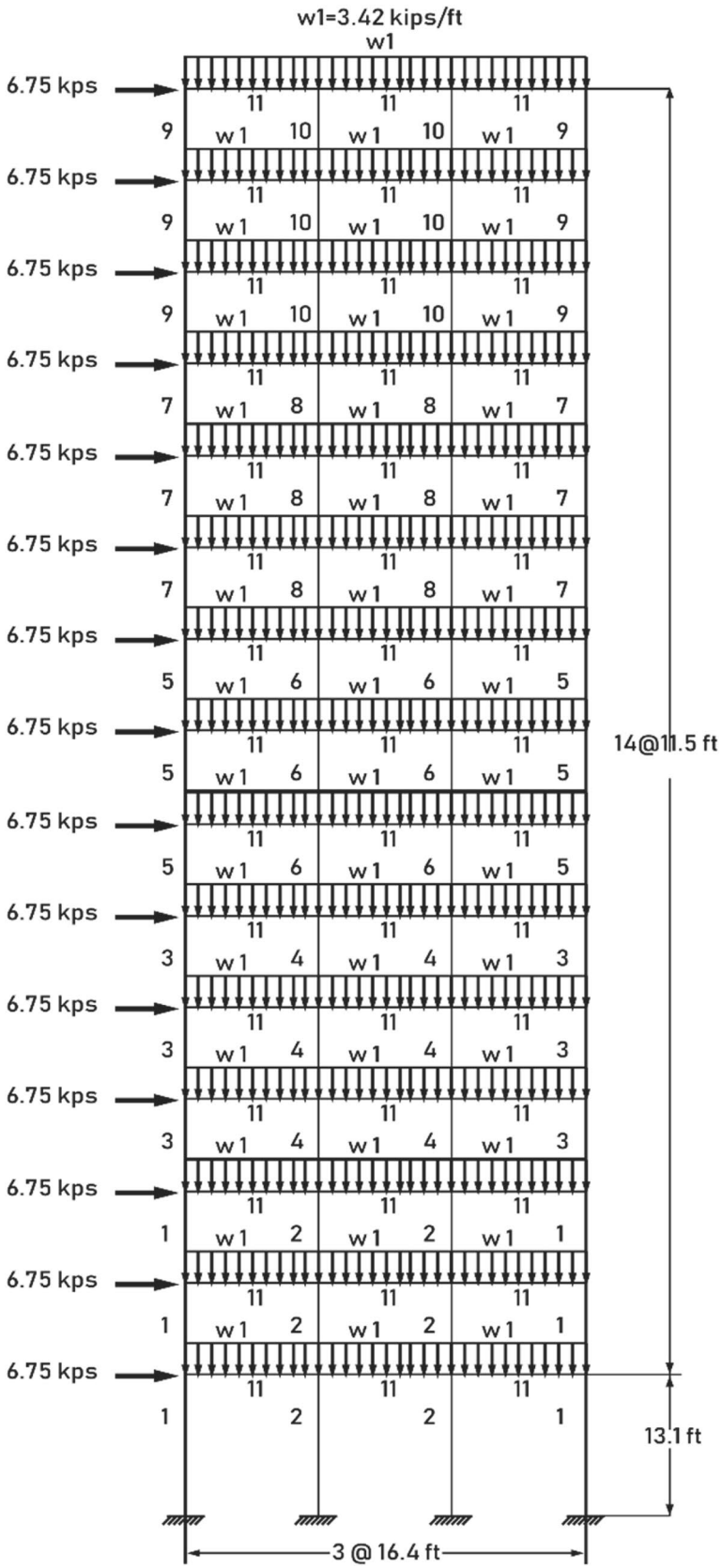


**Fig. 16** Schematic of the 3-bay 15-story frame

**Table 10** Comparison of the optimized design of the 3-bay 15-story obtained by different algorithms

| Element type | Area of cross sections ($in^2$) | | | |
|---|---|---|---|---|
| | VPS (Kaveh and Ilchi 2016) | CBO (Kaveh and Ilchi 2016) | TLBO | BHMO |
| 1 | 32.7 | 34.4 | 43.2 | 29.1 |
| 2 | 47.4 | 38.8 | 47.4 | 47.4 |
| 3 | 25.9 | 28.2 | 25.6 | 24.8 |
| 4 | 35.1 | 35.1 | 30.6 | 30.6 |
| 5 | 24.3 | 27.3 | 22.3 | 20.0 |
| 6 | 30.6 | 28.5 | 30.6 | 25.3 |
| 7 | 16.7 | 22.3 | 20.0 | 13.0 |
| 8 | 33.5 | 19.1 | 17.9 | 20.0 |
| 9 | 9.71 | 17.6 | 10.3 | 9.1 |
| 10 | 13.5 | 11.5 | 9.71 | 13.3 |
| 11 | 13.0 | 14.7 | 13.0 | 13.0 |
| Total weight (lb) | 101,385 | 99,623 | 97,149 | 87,925 |

**Table 11** Comparison of the optimized design of the 3-bay 15-story obtained by different algorithms

| Element type | Type of cross sections | | | |
|---|---|---|---|---|
| | VPS (Kaveh and Ilchi 2016) | CBO (Kaveh and Ilchi 2016) | TLBO | BHMO |
| 1 | W 21×111 | W 24×117 | W 21×147 | W 14×99 |
| 2 | W 27×161 | W 21×132 | W 27×161 | W 27×161 |
| 3 | W 10×88 | W 12×96 | W 12×87 | W 27×84 |
| 4 | W 18×119 | W 18×119 | W 24×104 | W 24×104 |
| 5 | W 21×83 | W 21×93 | W 18×76 | W 21×68 |
| 6 | W 24×104 | W 18×97 | W 24×104 | W 18×86 |
| 7 | W 21×57 | W 18×76 | W 21×68 | W 21×44 |
| 8 | W 27×114 | W 18×65 | W 14×61 | W 21×68 |
| 9 | W 10×33 | W 18×60 | W 18×35 | W 8×31 |
| 10 | W 18×46 | W 10×39 | W 10×33 | W 16×45 |
| 11 | W 21×44 | W 21×50 | W 21×44 | W 21×44 |

(248.2 MPa). The effective length factors of the members are calculated as $k_x \geq 0$ for a sway-permitted frame, and the out-of-plane effective length factor is specified as $k_y = 1.0$. Each column is considered as non-braced along its length, and the non-braced length for each beam member is specified as one-fifth of the span length. Tables 10 and 11 contain the calculated values in detail.

**Optimum design of 3-bay 24-story frame problem** Figure 17 shows the schematic of a 3-bay 24-story frame with its loading conditions. W14 sections are considered for 16 column element groups sections, while the four beam element groups are chosen from all 267 W-shapes. The yield stress of steel and the modulus of elasticity are taken as 33.4 ksi (230.3 MPa) and 29.732 Msi (205 GPa), respectively. The effective length factors of the members are calculated as $k_x \geq 0$ for a sway-permitted frame, and the out-of-plane effective length factor is specified as $k_y = 1.0$. All columns and beams are considered as non-braced along their lengths. The comparison of the optimized design obtained by different algorithms is reported in Tables 12 and 13.

## Concluding remarks

In this paper, a new meta-heuristic algorithm is proposed that covers the drawbacks of the other well-known methods using two novel techniques. The first is a powerful mathematical kernel, which (1) finds the optimum direction of each variable for changing and (2) directs them to the best position. For both purposes, the covariance matrix is calculated for each variable and cost function in each iteration. The second novelty is an appropriate physical simulation (based on the mechanics of the black holes). It controls the update of variables and the elimination of weakly generated data in each iteration. According to these two novelties, the proposed algorithm finds the global best more economically and faster than the other methods. According to the calculation of covariance matrix in each iteration, for large-scale problems it is necessary to define some complementary tricks to jumping some fundamental steps and increase the converge rate of algorithm.Finally, the efficiency and potency of the new method are investigated by solving several examples from two categories. The first consists of 17 mathematical benchmark problems, in which the optimum solutions are analytically available. The algorithm found the optimum solution in the first category in low-level computational costs (time and memory). The second category contains four real-size with real-loading conditions structural engineering problems in which the best designs are obtained by the Black Hole Mechanics Optimization Algorithm. In both relevant sections ("Benchmark optimization problems" and "Structural engineering examples"), the results are compared with some other recently developed algorithms, illustrating the efficiency, potency, and applicability of the new algorithm.

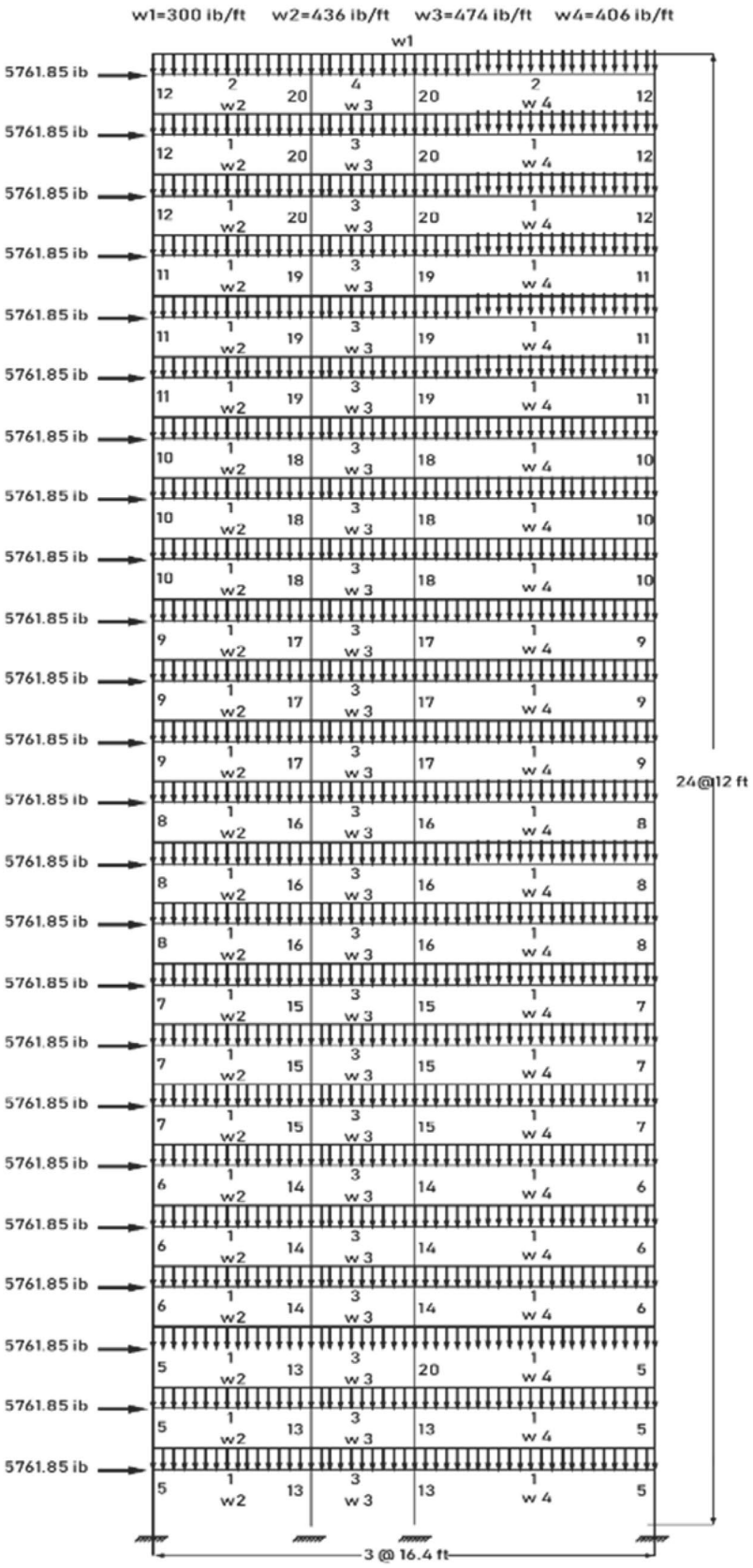


**Fig. 17** Schematic of the 3-bay 24-story frame

**Table 12** Comparison of the optimized design of the 3-bay 24-story obtained by different algorithms

| Element type | Area of cross sections ($in^2$) | | | |
|---|---|---|---|---|
| | VPS (Kaveh and Ilchi 2016) | CBO (Kaveh and Ilchi 2016) | TLBO | BHMO |
| 1 | 52.3 | 52.3 | 52.3 | 52.3 |
| 2 | 5.3 | 6.5 | 8.84 | 8.84 |
| 3 | 16.2 | 16.2 | 16.2 | 16.2 |
| 4 | 6.2 | 4.7 | 8.3 | 2.7 |
| 5 | 38.8 | 38.8 | 32 | 38.8 |
| 6 | 38.8 | 38.8 | 38.8 | 29.1 |
| 7 | 38.8 | 38.8 | 35.3 | 35.3 |
| 8 | 38.8 | 32 | 21.8 | 21.8 |
| 9 | 20.0 | 24.1 | 21.8 | 21.8 |
| 10 | 15.6 | 21.8 | 20.0 | 12.6 |
| 11 | 12.6 | 10.0 | 8.85 | 8.85 |
| 12 | 12.6 | 6.49 | 11.2 | 6.49 |
| 13 | 43.2 | 43.2 | 43.2 | 26.5 |
| 14 | 43.2 | 38.8 | 38.8 | 35.3 |
| 15 | 35.3 | 32.0 | 29.1 | 26.5 |
| 16 | 26.5 | 24.1 | 24.1 | 29.1 |
| 17 | 26.5 | 17.9 | 20.0 | 20.0 |
| 18 | 17.9 | 14.1 | 14.1 | 17.9 |
| 19 | 8.85 | 8.85 | 10.0 | 12.6 |
| 20 | 7.69 | 6.49 | 6.49 | 6.49 |
| Total weight (lb) | 239,942 | 226,067 | 218,599 | 203,427 |

**Table 13** Comparison of the optimized design of the 3-bay 24-story obtained by different algorithms

| Element type | Type of cross sections | | | |
|---|---|---|---|---|
| | VPS (Kaveh and Ilchi 2016) | CBO (Kaveh and Ilchi 2016) | TLBO | BHMO |
| 1 | W 27×178 | W 27×178 | W 27×178 | W 27×178 |
| 2 | W 8×18 | W 12×22 | W 10×30 | W 10×30 |
| 3 | W 24×55 | W 24×55 | W 24×55 | W 24×55 |
| 4 | W 8×21 | W 12×16 | W 8×28 | W 6×9 |
| 5 | W 21×132 | W 21×132 | W 14×109 | W 21×132 |
| 6 | W 21×132 | W 21×132 | W 21×132 | W 14×99 |
| 7 | W 21×132 | W 21×132 | W 14×120 | W 14×120 |
| 8 | W 21×132 | W 14×109 | W 14×74 | W 14×74 |
| 9 | W 21×68 | W 14×82 | W 14×74 | W 14×74 |
| 10 | W 14×53 | W 14×74 | W 21×68 | W 14×43 |
| 11 | W 14×43 | W 14×34 | W 14×30 | W 14×30 |
| 12 | W 14×43 | W 14×22 | W 14×38 | W 14×22 |
| 13 | W 21×147 | W 21×147 | W 21×147 | W 14×90 |
| 14 | W 21×147 | W 21×132 | W 21×132 | W 14×120 |
| 15 | W 14×120 | W 14×109 | W 14×99 | W 14×90 |
| 16 | W 14×90 | W 14×82 | W 14×82 | W 14×99 |
| 17 | W 14×90 | W 14×61 | W 21×68 | W 21×68 |
| 18 | W 14×61 | W 14×48 | W 14×48 | W 14×61 |
| 19 | W 14×30 | W 14×30 | W 14×34 | W 14×43 |
| 20 | W 14×26 | W 14×22 | W 14×22 | W 14×22 |

## Compliance with ethical standards

**Conflict of interest** No potential conflict of interest was reported by the authors.

## References


American Institute of Steel Construction (AISC). (1989). *Manual of steel construction: Allowable stress design*. Chicago: American Institute of Steel Construction.

American Institute of Steel Construction (AISC). (2001). *Manual of steel construction: Load resistance factor design*. Chicago: American Institute of Steel Construction.

Askarzadeh, A., & Rezazadeh, A. (2013). A new heuristic optimization algorithm for modeling of proton exchange membrane fuel cell: Bird mating optimizer. *International Journal of Energy Research, 37*(10), 1196–1204. https://doi.org/10.1002/er.2915.

Atashpaz-Gargari, E., & Lucas, C. (2007). Imperialist competitive algorithm: An algorithm for optimization inspired by imperialistic competition. *IEEE Congress on Evolutionary Computation*. https://doi.org/10.1109/CEC.2007.4425083.

Balochian, S., & Baloochian, H. (2019). Social mimic optimization algorithm and engineering applications. *Expert Systems with Applications, 134*, 178–191. https://doi.org/10.1016/j.eswa.2019.05.035.

Bekenstein, J. D. (1973). Black holes and entropy. *Physical review D: Particles and Fields, 7*(8), 2333. https://doi.org/10.1103/PhysRevD.7.2333.

Carroll, S. (2019). *Spacetime and geometry: An introduction to general relativity*. Cambridge: Cambridge University Press. https://doi.org/10.1017/9781108770385.

Carvalho, J., Lemonge, A., Carvalho, E., Hallak, P., & Bernardino, H. (2017). Truss optimization with multiple frequency constraints and automatic member grouping. *Structural and Multidisciplinary Optimization*. https://doi.org/10.1007/s00158-017-1761-x.

Chen, W., Zhang, J., Lin, Y., Chen, N., Zhan, Z.-H., Chung, H. S., et al. (2013). Particle swarm optimization with an aging leader and challengers. *IEEE Transactions on Evolutionary Computation, 17*, 241–258. https://doi.org/10.1109/TEVC.2011.2173577.

Davies, P. C. (1978). Thermodynamics of black holes. *Reports on Progress in Physics, 41*(8), 1313. https://doi.org/10.1088/0034-4885/41/8/004.

Dorigo, M., Maniezzo, V., & Colorni, A. (1996). Ant system: optimization by a colony of cooperating agents. *IEEE Transactions Systems, Man, and Cybernetics, Part B (Cybernetics), 26*(1), 29–41. https://doi.org/10.1109/3477.484436.

Du, D.-C., Vinh, H.-H., Trung, V.-D., Hong Quyen, N.-T., & Trung, N.-T. (2018). Efficiency of Jaya algorithm for solving the optimization-based structural damage identification problem based on a hybrid objective function. *Engineering Optimization, 50*(8), 1233–1251. https://doi.org/10.1080/0305215X.2017.1367392.

Dumonteil, P. (1992). Simple equations for effective length factors. *Engineering Journal AISC, 29*(3), 111–115.
Erol, O. K., & Eksin, I. (2006). A new optimization method: Big bang–big crunch. *Advances in Engineering Software, 37*(2), 106–111. https://doi.org/10.1016/j.advengsoft.2005.04.005.
Eskandar, H., Sadollah, A., Bahreininejad, A., & Hamdi, M. (2012). Water cycle algorithm—A novel metaheuristic optimization method for solving constrained engineering optimization problems. *Computers & Structures, 110*, 151–166. https://doi.org/10.1016/j.compstruc.2012.07.010.
Ferreira, M. P., Rocha, M. L., Silva Neto, A. J., & Sacco, W. F. (2018). A constrained ITGO heuristic applied to engineering optimization. *Expert Systems with Applications, 110*, 106–124. https://doi.org/10.1016/j.eswa.2018.05.027.
Gandomi, A. H., & Alavi, A. H. (2012). Krill herd: a new bio-inspired optimization algorithm. *Communications in Nonlinear Science and Numerical Simulation, 17*(12), 4831–4845. https://doi.org/10.1016/j.cnsns.2012.05.010.
Garey, M., & Johnson, D. (1979). Computer and intractability: A guide to the theory of NP-Completeness. Freeman, San Francisco, Chapters 1–3. https://doi.org/10.1137/1024022.
Geem, Z. W., Kim, J. H., & Loganathan, G. V. (2001). A new heuristic optimization algorithm: Harmony search. *Simulation, 76*(2), 60–68. https://doi.org/10.1177/003754970107600201.
Glover, F. (1989). Tabu search—part I. *Informs Journal on Computing, 1*(3), 190–206. https://doi.org/10.1287/ijoc.1.3.190.
Got, A., Moussaoui, A., & Zouache, D. (2019). A guided population archive whale optimization algorithm for solving multiobjective optimization problems. *Expert Systems with Applications, 141*, 112972. https://doi.org/10.1016/j.eswa.2019.112972.
Hawking, S. W., & Ellis, G. F. R. (1971). Gravitational radiation from colliding black holes. *Physical Review Letters, 26*(21), 1344. https://doi.org/10.1103/PhysRevLett.26.1344.
Hawking, S. W., & Ellis, G. F. R. (1973). *The large scale structure of space-time* (Vol. 1). Cambridge: Cambridge University Press.
Hawking, S. W., & Ellis, G. F. R. (1974a). Black hole explosions? *Nature, 248*(5443), 30. https://doi.org/10.1038/248030a0.
Hawking, S. W., & Ellis, G. F. R. (1974b). *Nature, 248*(30), 199.
Hawking, S. W., & Ellis, G. F. R. (1990). Book review: The illustrated a brief history of time. *Sky Telescope*. *Journal of Near-Death Studies, 9*(2). https://doi.org/10.17514/jnds-1990-9-2-p123-131.
Holland, J. H. (1992). Genetic algorithms. *Scientific American, 267*(1), 66–73. https://doi.org/10.1038/scientificamerican0792-66.
Kalinin, M., & Kononogov, S. (2005). Boltzmann's constant, the energy meaning of temperature, and thermodynamic irreversibility. *Measurement Techniques, 48*(7), 632–636. https://doi.org/10.1007/s11018-005-0195-9.
Karaboga, D., & Basturk, B. (2007). A powerful and efficient algorithm for numerical function optimization: Artificial bee colony (ABC) algorithm. *Journal of Global Optimization, 39*(3), 459–471. https://doi.org/10.1007/s10898-007-9149-x.
Kaveh, A. (2017). *Advances in metaheuristic algorithms for optimal design of structures, Chapter on Tug of war optimization* (pp. 451–487). Cham: Springer. https://doi.org/10.1007/978-3-319-46173-1_15.
Kaveh, A., & Bakhshpoori, T. (2016). Water evaporation optimization: A novel physically inspired optimization algorithm. *Computers & Structures, 167*, 69–85. https://doi.org/10.1016/j.compstruc.2016.01.008.
Kaveh, A., & Bolandgerami, A. (2016). Optimal design of large-scale space steel frames using cascade enhanced colliding body optimization. *Structural and Multidisciplinary Optimization*. https://doi.org/10.1007/s00158-016-1494-2.
Kaveh, A., & Farhoudi, N. (2013). A new optimization method: Dolphin echolocation. *Advances in Engineering Software, 59*, 53–70. https://doi.org/10.1016/j.advengsoft.2013.03.004.
Kaveh, A., & Ilchi Ghazaan, M. (2015). A comparative study of CBO and ECBO for optimal design of skeletal structures. *Computers and Structures, 153*, 137–147. https://doi.org/10.1016/j.compstruc.2015.02.028.
Kaveh, A., & Ilchi Ghazaan, M. (2017a). Enhanced whale optimization algorithm for sizing optimization of skeletal structures. *Mechanics Based Design of Structures and Machines, 45*(3), 345–362. https://doi.org/10.1080/15397734.2016.1213639.
Kaveh, A., & Ilchi Ghazaan, M. (2017b). Vibrating particles system algorithm for truss optimization with multiple natural frequency constraints. *Acta Mechanica, 228*(1), 307–322. https://doi.org/10.1007/s00707-016-1725-z.
Kaveh, A., & Khayatazad, M. (2012). A new meta-heuristic method: Ray optimization. *Computers & Structures, 112*, 283–294. https://doi.org/10.1016/j.compstruc.2012.09.003.
Kaveh, A., Lakinejad, K., & Alinejad, B. (2012). Performance-based multi-objective optimization of large steel structures. *Acta Mechanica, 223*(2), 355–369. https://doi.org/10.1007/s00707-011-0564-1.
Kaveh, A., & Mahdavi, V. R. (2013). Optimal design of structures with multiple natural frequency constraints using a hybridized BB-BC/Quasi-Newton algorithm. *Periodica Polytechnica Civil Engineering, 57*(1), 27–38. https://doi.org/10.3311/PPci.2139.
Kaveh, A., & Mahdavi, V. R. (2015). *Colliding bodies optimization*. Cham: Springer. https://doi.org/10.1007/978-3-319-19659-6.
Kaveh, A., Mehdipour, R., & Javadi, S. M. (2019). Optimum design of large steel skeletal structures using chaotic firefly optimization algorithm based on the Gaussian map. *Structural and Multidisciplinary Optimization, 60*(3), 879–894. https://doi.org/10.1007/s00158-019-02263-1.
Kaveh, A., Mirzaei, K., & Jafarvand, A. (2015). An improved magnetic charged system search for optimization of truss structures with continuous and discrete variables. *Applied Soft Computing, 28*(C), 400–410. https://doi.org/10.1016/j.asoc.2014.11.056.
Kaveh, A., & Talatahari, S. (2010a). A novel heuristic optimization method: Charged system search. *Acta Mechanica, 213*(3–4), 267–289. https://doi.org/10.1007/s00707-009-0270-4.
Kaveh, A., & Talatahari, S. (2010b). Optimum design of skeletal structures using imperialist competitive algorithm. *Computers & Structures, 88*, 1220–1229. https://doi.org/10.1016/j.compstruc.2010.06.011.
Hasancebi, O., & Kazemzadeh Azad, S. (2015). Adaptive dimensional search: A new metaheuristic algorithm for discrete truss sizing optimization. *Computers & Structures*. https://doi.org/10.1016/j.compstruc.2015.03.014.
Kazemzadeh Azad, S. (2019). Monitored convergence curve: A new framework for metaheuristic structural optimization algorithms. *Structural and Multidisciplinary Optimization*. https://doi.org/10.1007/s00158-019-02219-5.
Kennedy, J., & Eberhart, R. (1995). Particle swarm optimization (PSO). Paper presented at the Proc. *IEEE International Conference on Neural Networks*, Perth, Australia. https://doi.org/10.1109/ICNN.1995.488968
Kirkpatrick, S., Gelatt, C. D., & Vecchi, M. P. (1983). Optimization by simulated annealing. *Science, 220*(4598), 671–680. https://doi.org/10.1126/science.220.4598.671.
Latif, M. A., & Saka, M. P. (2019). Optimum design of tied-arch bridges under code requirements using enhanced artificial bee colony algorithm. *Advances in Engineering Software, 135*, 102685. https://doi.org/10.1016/j.advengsoft.2019.102685.
Lewis, G. F., & Kwan, J. (2007). No way back: Maximizing survival time below the Schwarzschild event horizon. *Publications of the Astronomical Society of Australia, 24*(2), 46–52. https://doi.org/10.1071/AS07012.

Mirjalili, S. (2015). The ant lion optimizer. *Advances in Engineering Software, 83*, 80–98. https://doi.org/10.1016/j.advengsoft.2015.01.010.

Mirjalili, S., & Lewis, A. (2016). The whale optimization algorithm. *Advances in Engineering Software, 95*, 51–67. https://doi.org/10.1016/j.advengsoft.2016.01.008.

Mirjalili, S., Mirjalili, S. M., & Lewis, A. (2014). Grey wolf optimizer. *Advances in Engineering Software, 69*, 46–61. https://doi.org/10.1016/j.advengsoft.2013.12.007.

Moosavian, N., & Kasaee Roodsari, B. (2014). Soccer league competition algorithm: A novel meta-heuristic algorithm for optimal design of water distribution networks. *Swarm and Evolutionary Computation, 17*, 14–24. https://doi.org/10.1016/j.swevo.2014.02.002.

Mucherino, A., & Seref, O. (2007). Monkey search: A novel metaheuristic search for global optimization. *Paper presented at the AIP conference proceedings*. https://doi.org/10.1063/1.2817338.

Park, K. (2018). *Fundamentals of probability and stochastic processes with applications to communications*. Berlin: Springer. https://doi.org/10.1007/978-3-319-68075-0.

Planck, M. (1899). Natürliche Maßeinheiten. *Der Königlich Preussischen Akademie Der Wissenschaften*. https://doi.org/10.1017/CBO9780511524646.

Rao, R. V., Savsani, V. J., & Vakharia, D. P. (2011). Teaching–learning-based optimization: A novel method for constrained mechanical design optimization problems. *Computer-Aided Design, 43*(3), 303–315. https://doi.org/10.1016/j.cad.2010.12.015.

Rechenberg, I. (1978). *Evolutionstrategie 1 lab course*. Berlin, Springer, Heidelberg, ISBN 978-3-642-69542-1. https://doi.org/10.1007/978-3-642-69540-7-13.

Rice, J. A. (2006). *Mathematical statistics and data analysis: Cengage learning*. Cambridge University. https://doi.org/10.2307/3619963.

Russo, I. L. S., Bernardino, H. S., & Barbosa, H. J. C. (2017). Knowledge discovery in multiobjective optimization problems in engineering via Genetic Programming. *Expert Systems with Applications, 99*, 93–102. https://doi.org/10.1016/j.eswa.2017.12.008.

Schutz, B. (2003). *Gravity from the ground up: An introductory guide to gravity and general relativity*. Cambribge: Cambridge University Press.

Shah-Hosseini, H. (2011). Principal components analysis by the galaxy-based search algorithm: A novel metaheuristic for continuous optimisation. *International Journal of Computational Science and Engineering, 6*(1–2), 132–140. https://doi.org/10.1504/IJCSE.2011.041221.

Shapiro, S. L., Teukolsky, S. A., & Winicour, J. (1995). Toroidal black holes and topological censorship. *Physical review D: Particles and Fields, 52*(12), 6982–6987. https://doi.org/10.1103/physrevd.52.6982.

Storn, R., & Price, K. (1997). Differential evolution—a simple and efficient heuristic for global optimization over continuous spaces. *Journal of Global Optimization, 11*(4), 341–359. https://doi.org/10.1023/A:1008202821328.

Suganthan, P., Hansen, N., Liang, J., Deb, K., Chen, Y. P., Auger, A., et al. (2005). Problem definitions and evaluation criteria for the CEC 2005 special session on real-parameter optimization. *Natural Computing, 13*, 341–357.

Talbi, E. (2009). *Metaheuristics: from design to implementation* (Vol. 74). Hoboken: Wiley. https://doi.org/10.1002/9780470496916.

Taylor, E. F., & Wheeler, J. A. (2000). *Exploring black holes* (Vol. 98). San Francisco: Addison Wesley Longman.

Tejani, G. G., Pholdee, N., Bureerat, N., Prayogo, D., & Gandomi, A. H. (2019). Structural optimization using multi-objective modified adaptive symbiotic organisms search. *Expert Systems with Applications, 125*, 425–441. https://doi.org/10.1016/j.eswa.2019.01.068.

Truong, V. H., & Kim, S. E. (2018). Reliability-based design optimization of nonlinear inelastic trusses using improved differential evolution algorithm. *Advances in Engineering Software, 121*, 59–74. https://doi.org/10.1016/j.advengsoft.2018.03.006.

Wald, R. M. (1999). Gravitational collapse and cosmic censorship. *Black holes, gravitational radiation and the universe* (pp. 69–86). Berlin: Springer.

Wald, R. M. (2001). The thermodynamics of black holes. *Living Reviews in Relativity, 4*(1), 6. https://doi.org/10.12942/lrr-2001-6.

Yang, X.-S. (2010a). *A new metaheuristic bat-inspired algorithm. In Nature inspired cooperative strategies for optimization (NICSO 2010)* (pp. 65–74). Berlin: Springer. https://doi.org/10.1007/978-3-642-12538-6_6.

Yang, X.-S. (2010b). Firefly algorithm, stochastic test functions and design optimization. *International Journal of Bio-Inspired Computation*. https://doi.org/10.1504/IJBIC.2010.032124.

Yang, X.-S., & Deb, S. (2009). *Cuckoo search via Lévy flights.* Paper presented at the 2009 World Congress on Nature & Biologically Inspired Computing (NaBIC). https://doi.org/10.1109/NABIC.2009.5393690

Zheng, T., Luo, W., Hou, R., Lu, Z., & Cui, J. (2019). A novel experience-based learning algorithm for structural damage identification: Simulation and experimental verification. *Engineering Optimization*. https://doi.org/10.1080/0305215X.2019.1668935.